ORIGINAL ARTICLES

SPECTROSCOPIC STUDY OF METHYLENE BLUE IN VIVO: EFFECTS ON TISSUE OXYGENATION AND TUMOR METABOLISM

Pominova D.V.[1,2], **Ryabova A.V.**[1,2], **Skobeltsin A.S**[1], **Markova I.V.**[2], **Romanishkin I.D.**[1], **Loschenov V.B.**[1,2]
[1]Prokhorov General Physics Institute of Russian Academy of Sciences, Moscow, Russia
[2]National Research Nuclear University MEPhI (Moscow Engineering Physics Institute), Moscow, Russia

Abstract

Methylene blue (MB) is a promising photosensitizer (PS) for the treatment of pathological neoplasms, since it has both photodynamic activity (under laser irradiation) and redox and catalytic properties (in the absence of light). In the framework of this work, using spectroscopic methods, the effect of intravenous administration of MB on tissue oxygenation of hemoglobin in small animals in vivo in tumor and normal tissues was analyzed. The influence of MB on cell metabolism was analyzed. It has been shown that the use of MB promotes an increase in oxygen consumption by the tumor, and also leads to a shift in metabolism towards oxidative phosphorylation. It was shown that the use of MB contributes to an increase in oxygen consumption by the tumor, and also leads to a shift in metabolism towards oxidative phosphorylation.

Keywords: methylene blue, oxygenation, tumor metabolism.

For citations: Pominova D.V., Ryabova A.V., Skobeltsin A.S., Markova I.V., Romanishkin I.D., Loschenov V.B., Spectroscopic study of methylene blue *in vivo*: effects on tissue oxygenation and tumor metabolism, *Biomedical Photonics*, 2023, vol. 12, no. 1, pp. 4–13. doi: 10.24931/2413–9432–2023–12–1-4-13.

Contacts: Pominova D.V., e-mail: pominovadv@gmail.com

СПЕКТРОСКОПИЧЕСКОЕ ИССЛЕДОВАНИЕ МЕТИЛЕНОВОГО СИНЕГО IN VIVO: ВЛИЯНИЕ НА ОКСИГЕНАЦИЮ ТКАНЕЙ И ОПУХОЛЕВЫЙ МЕТАБОЛИЗМ

Д.В. Поминова[1,2], **А.В. Рябова**[1,2], **А.С. Скобельцин**[1], **И.В. Маркова**[2], **И.Д. Романишкин**[1], **В.Б. Лощенов**[1,2]
[1]Институт общей физики им. А. М. Прохорова Российской академии наук, Москва, Россия
[2]Национальный исследовательский ядерный университет «МИФИ», Москва, Россия

Резюме

Метиленовый синий (МС) является перспективным фотосенсибилизатором для терапии патологических новообразований, поскольку обладает как фотодинамической активностью (при лазерном облучении), так и окислительно-восстановительными и каталитическими свойствами (в отсутствии света). В рамках данной работы при помощи спектроскопических методов было проанализировано влияние внутривенного введения МС на тканевую оксигенацию гемоглобина на малых животных *in vivo* в опухоли и нормальных тканях. Проведен анализ влияния МС на клеточный метаболизм. Показано, что применение МС способствует увеличению потребления кислорода опухолью, а также приводит к сдвигу метаболизма в сторону окислительного фосфорилирования.

Ключевые слова: метиленовый синий, оксигенация, опухолевый метаболизм

Для цитирования: Поминова Д.В., Рябова А.В., Скобельцин А.С., Маркова И.В., Романишкин И.Д., Лощенов В.Б. Спектроскопическое исследование метиленового синего *in vivo*: влияние на оксигенацию тканей и опухолевый метаболизм // Biomedical Photonics. – 2023. – Т. 12, № 1. – С. 4–13. doi: 10.24931/2413–9432–2023–12–1-4-13.

Контакты: Поминова Д.В.., e-mail: pominovadv@gmail.com

Introduction

Cancer is currently one of the major health problems in all developed and many developing countries of the world [1]. In this regard, a large number of publications are devoted to the study of the processes of tumor growth and their metastasis. To date, it is known that the tumor and its microenvironment are highly heterogeneous [2]. Cancer cells establish metabolic cross-talk with cellular and non-cellular components of the tumor microenvironment, which leads to the reorientation of immune cells to protect the tumor, provides cancer cells with the nutrients and promotes proliferation, invasion, metastasis, aggressiveness, resistance of tumors to treatment [3-6].

One of the driving forces of metabolic reprogramming is hypoxia and a cascade of biochemical reactions leading to local acidification. Growing tumors are characterized by insufficient blood perfusion, hypoxia, inflammation, enhanced fatty acid metabolism, nucleotide synthesis and glutaminolysis [7]. The hallmarks of tumor cell metabolism are a high level of glycolysis and a low level of oxidative phosphorylation, even when oxygen is present in the tissues in sufficient quantities. Most cancer cells produce lactic acid (lactate), a characteristic product of glycolysis [8]. Lactate has a critical function in signaling, through inducing the expression of vascular endothelial growth factor and the polarization of tumor-associated macrophages and induce expression of arginase 1 by macrophages, which has an important role in tumor growth [9]. Local acidity is a central regulator of cancer immunity that orchestrates both local and systemic immunosuppression [7]. Low oxygen supply to the tumor further enhances glycolysis, which in turn causes the expression of hypoxia-inducible factor 1α (HIF-1α) and mediates the effects of lactic acid.

An urgent task is to search for new approaches for the treatment of cancer, which are aimed at correcting the functional state of the tumor microenvironment [10-11]. One promising approach is photodynamic therapy (PDT) [12]. PDT uses a special drug–PS, which under the action of light generates reactive oxygen species that not only damage biological structures, but are also natural regulators of cell proliferation, metabolism, and apoptosis [13-14]. In recent years PDT has been increasingly used to treat tumors of various localizations. In Russia, a large number of scientific groups are engaged in the development of PDT methods [15-19]. PDT has a number of advantages over other methods: it is effective against all types of tumors; if necessary, the procedure can be repeated many times, since there are no cumulative toxic effects and acquired resistance; the procedure is carried out on an outpatient basis, provides a good cosmetic effect and can be used even for the elderly and debilitated people. The effectiveness and safety of PDT have been proven by numerous clinical studies and active practical use [20-22]. A problem for PDT is the effect on tumors that are in a state of hypoxia, for example, many tumors of the prostate and pancreas.

One of the interesting PS is MB, which, in addition to fluorescence in the red part of the spectrum and significant photodynamic activity, has redox and catalytic properties. In the 1930s, MB was actively researched [23-26] to counteract the effects of cyanide intoxication, however, after the advent of other antidotes [27], research on its mechanisms of action and effectiveness was abandoned for decades. According to a pioneering work [28], MB increases oxygen consumption by tissues with aerobic glycolysis and tumors, while the effect of MB is approximately proportional to the enzymatic capacity of tissues. There is no effect on oxygen consumption by those normal tissues that do not have aerobic glycolysis. The catalytic properties of MB in relation to tumors are due to its interaction with lactic acid, which is formed as a result of aerobic glycolysis.

When released into the blood, MB is readily reduced to its colorless leuco form, leucomethylene blue (LMB). Reducing agents can be NAD(P)H [29-30] or reduced glutathione [31], the concentration of which decreases as a result of interaction with MB [32], and MB acquires electrons in the process. LMB, in turn, can be reoxidized to MB by molecules with a higher redox potential (such as O_2 or most metal compounds), donating electrons in the process, and a new reduction cycle can be initiated [32]. There is evidence that MB interacts directly with the mitochondrial electronic circuit, donating electrons to complexes I and III and/or providing partial restoration of the Krebs cycle [33], whenever NADH is oxidized by MB or even resuscitation of the mitochondrial electronic circuit. A positive effect of MB on peripheral blood flow has also been reported [34]. In clinical practice, MB is used to treat methemoglobinemia, since MB is able to reduce the ferrous iron in methemoglobin (the oxidized form of hemoglobin that is unable to carry oxygen) to the ferric state corresponding to normal hemoglobin [35] and also as an antidote for carbon monoxide poisoning. The MB/LMB pair quickly diffuses into the cytoplasm and mitochondria of any cells, including neurons [36], and can have different effects depending on the concentration of the redox state of its immediate environment. MB and LMB have different absorption peaks: LMB predominantly absorb in the UV region (256 nm), while MB has two absorption peaks in the UV and visible range (294 and 665 nm, respectively) [37]. There is also a semi-reduced form (radical) with an absorption maximum at a wavelength of 420 nm. This makes it possible to study MBs by spectroscopic methods and directly observe the transition of MB into LMB.

It should be noted that early studies of MB were carried out *ex vivo* using micromanometric methods. More recent studies have mostly been conducted in

cell cultures and have been indirect. Therefore, this work was devoted to the direct observation of the pharmacokinetics of MB *in vivo*, the study of the MB/LMB transition, and the assessment of the effect of MB on oxygenation and tumor metabolism using video fluorescence and spectroscopic methods. The present study was undertaken to characterize the metabolic responses to MB at various doses to determine the effects produced by the LMB/MB pair on cellular metabolism in a Lewis lung carcinoma (LLC) transplanted tumor mouse model. A spectroscopic study showed that with the accumulation of MB, there is a decrease in hemoglobin oxygenation in the tumor, which can be interpreted as an increase in oxygen consumption. Tissue cryosections were analyzed using fluorescence lifetime imaging microscopy (FLIM) in order to interpret intracellular metabolism in the areas of MB accumulation. It has been shown that there is a shift from glycolysis to oxidative phosphorylation after MB administration.

Materials and methods

Methylene blue

MB have been purchased at a pharmacy: "Methylene blue", an aqueous solution of 1%, the active substance methylthioninium chloride (OJSC "Samaramedprom").

Fluorescence imaging of MB in vivo

For the experiment, male BALB/c mice that were 25–30 g, 8–10 weeks old were used. The mice were kept at 21°C temperature in standard cages, the photoperiod was 12 hours of light and 12 hours of dark per day. The animals had access to standard laboratory feed and water *ad libitum*.

The LLC cell line of C57BL strain was used in experiments *in vivo* for tumor grafting. Inoculation of 50 μL of a 15% tumor cell suspension in Hanks' Balanced Salt Solution was performed intramuscularly on the right hind leg.

Experiments were performed on 14 after LLC cells injection. Tumor volume was determined by the measurement of two bisecting diameters in each tumor using calipers. The size of the tumor was determined by direct measurement of the tumor dimensions. The volume was calculated according to the equation: $V = (L \times W^2) \times 0.5$, where V = volume, L = length and W = width. All mice were divided into 2 groups depending on tumor size (small and large tumor, 50–75 and 100–150 mm^3 correspondingly). All measurements were triplicated.

MB was administered intravenously into the tail vein at a dose of 10 and 20 mg/kg with fluorescent control. Fluorescence was excited by laser radiation with a 660 nm wavelength.

Registration of fluorescent images was carried out using a black-and-white camera MQ013RG-ON (Ximea, Korea), with extended sensitivity in the near-infrared range, equipped with an interference filter that transmits in the range of 700-750 nm. The setup is shown in Fig. 1.

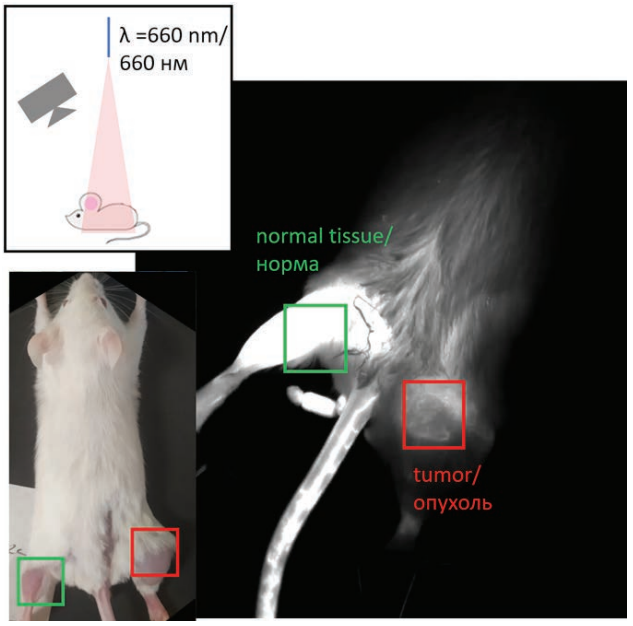

Рис. 1. Схематичное изображение расположения видеокамеры, источника лазерного излучения и мыши для флуоресцентной визуализации метиленового синего *in vivo*, фото животного с опухолью на правой лапе (красный квадрат) в обычном цвете и в флуоресцентном режиме.

Fig. 1. Schematic representation of the location of the video camera, laser source and mouse for fluorescence imaging of MB *in vivo*, photo of an animal with a tumor on the right paw (red square) in normal color and in fluorescent mode.

The fluorescent signal was recorded in a video file, which was further processed. After the injection of the dye, the mouse remained under laser irradiation for 5 minutes, during which the video file was recorded. The following method was used to assess pharmacokinetics from fluorescent images. For each frame of the recorded video file with a fluorescent signal, the average brightness in the specified area (tumor and normal tissue) was calculated. The brightness value in a pixel was normalized and took values from zero to one. Then, the time dependences of the average brightness of various zones of interest were plotted.

Study of methylene blue pharmacokinetics of using spectroscopic methods

Quantification of the MB accumulation in the tumor and in the normal tissue was carried out by spectroscopic methods using a fiber-optic spectrometer LESA-01-Biospec (Biospec, Russia). The device allows measurements of fluorescence spectra in the wavelength range of 350-1000 nm with a wavelength resolution of 3 nm. The exposure time for recording one spectrum can be varied in the range of 20 - 500 ms. To deliver and receive radiation, a fiber optic probe was used with

a central illuminating fiber supplying exciting laser radiation to the tissue and six peripheral fibers collecting scattered and fluorescent radiation. A helium-neon laser with a wavelength of 632.8 nm was used to excite MB fluorescence. The laser radiation power at the output of the fiber was 5 mW. A filter was installed at the entrance to the spectrometer to attenuate the laser radiation, which made it possible to observe its component backscattered by the tissue in the same dynamic range as the fluorescent radiation.

The assessment of the concentration of the drug in the tissues using a fiber-optic spectrometer is performed integrally, from the entire depth to which the laser signal penetrates. To quantitatively determine the MB concentration in organs and tissues, the calibration was performed using optical phantoms with an MB photosensitizer, which simulated the scattering and absorbing properties of biological tissues. Used MB concentrations of 0, 0.01, 0.05, 0.1, 0.5, 1, 2.5, 5 mg/kg were mixed with a scattering medium (1% fat emulsion Intralipid (Fresenius Kabi LLC, USA)) and put into tubes. The fluorescence spectra of optical phantoms with MB were recorded under excitation by a laser source with a wavelength of 632.8 nm. Based on the obtained spectra, the fluorescence index was determined for each optical phantom, equal to the ratio of the area under the MB fluorescence peak to the area under the scattered laser radiation peak. Using the calibration curve, a one-to-one correspondence is established between the fluorescence index of each of the phantoms and the concentration of MB in it. The calibration curve is then used to determine the concentration of MB *in vivo* from their measured fluorescence indices. Fluorescence index and MB concentration in optical phantoms were determined under the same external conditions. All measurements were carried out in a dark room without external light sources. Measurements were made at time points prior to administration, 10 minutes and 1 hour. For each time point, measurements were repeated three times for 3 animals.

Determination of hemoglobin oxygenation level in the tissue microvasculature by analyzing the diffuse reflectance spectra

The hemoglobin oxygenation measurement is based on the registration of diffuse reflectance spectra in the 500-600 nm wavelength spectral range, which makes it possible to quantify the concentration of hemoglobin in oxygenated and deoxygenated form. Fig. 2 shows the sketch of the experimental setup for diffuse reflectance spectra registration *in vivo* (Fig. 2a) and characteristic absorption spectra of oxygenated and deoxygenated hemoglobin forms (Fig. 2b).

A halogen lamp with a fiber optic output was used as a broadband radiation source. To receive radiation, a fiber with a diameter of 400 μm was used. The light supplied to the biological object passed through the tissue, experiencing scattering and absorption, and entered the receiving fiber. The receiving and transmitting fibers were in light contact with the test tissue in order to avoid affecting its optical properties when pressed. From the receiving fiber, light entered the LESA-01-BIOSPEC

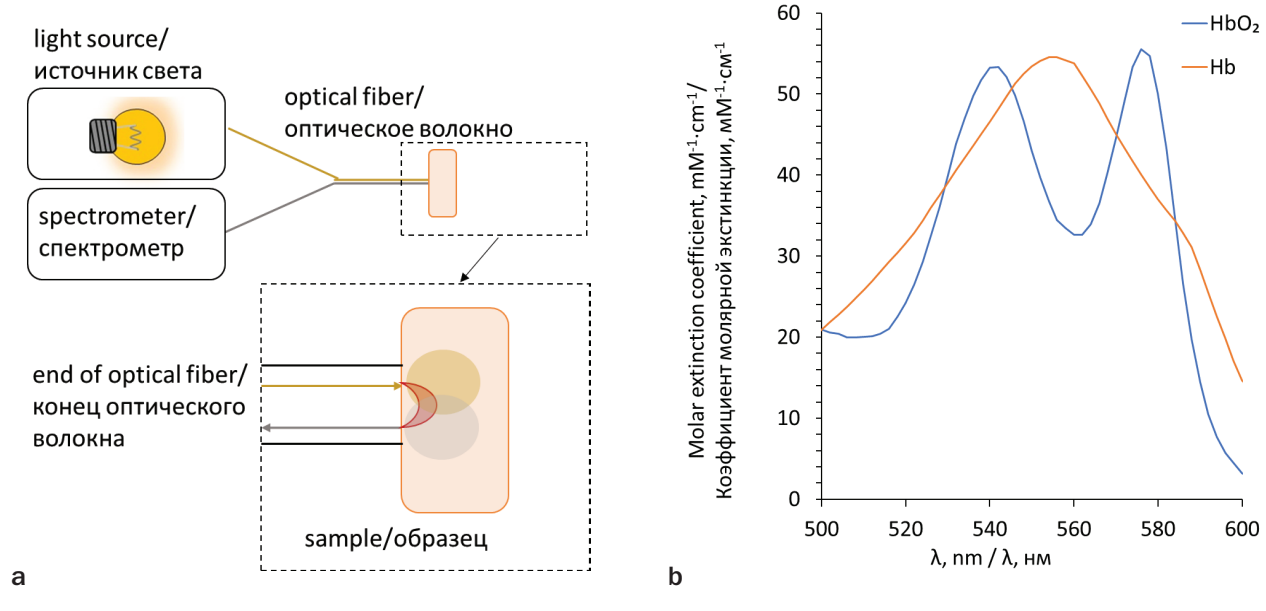

Рис. 2. Схема экспериментальной установки для измерения спектров обратного диффузного рассеяния *in vivo* (a) и характерические спектры поглощения оксигенированной и деоксигенированной форм гемоглобина (b).
Fig. 2. Scheme of the experimental setup for measuring diffuse reflectance spectra *in vivo* (a) and characteristic absorption spectra of oxygenated and deoxygenated hemoglobin forms (b).

laser spectrum analyzer (Biospec, Russia), which was controlled via a USB interface by a personal computer using special software Uno (Biospec, Russia), which was used to register and process the spectral dependencies. To eliminate the influence of the spectral sensitivity of the detector, the transmission spectrum of the fibers, and the spectral radiative characteristic of the light source on the detected signal, the measurements were carried out relative to a standard sample ($BaSO_4$) with a reflection coefficient close to unity in the spectral range of interest. The measurement technique is described in more detail in [38].

Cryosections preparation and analysis

After spectroscopic study mice were euthanized. Tumors along with subcutaneous tissue, skin and muscle were excised en bloc and frozen. Using a freezing microtome Microm HM 560 Cryostat (Thermo Scientific, Waltham, Massachusetts, USA) cryosections were prepared. Thickness was estimated to be 50 μm for the FLIM procedure and 100 μm for absorption spectra measurements. The sections were placed in saline under a coverslip and examined immediately using a laser scanning microscope in order to analyze the metabolic changes after MB accumulation. To study the absorption spectra, the sections were placed on quartz glasses. Registration of absorption spectra in the range of 200-1000 nm was carried out using a Hitachi U3400 spectrophotometer (Hitachi, Japan).

Assessment of intracellular metabolism by endogenous NADH photoluminescence lifetime using FLIM

To investigate the metabolic changes in the tissue, an approach based on calculating NADH fluorescence lifetime metabolic index was used [39]. Tissue sections were examined using an LSM-710-NLO laser scanning microscope (Carl Zeiss AG, Germany) with Plan-Apochromat 63x/1.4 Oil objective. NADH fluorescence was excited by 740 nm two-photon laser excitation using Chameleon Ultra II femtosecond laser (Coherent, USA). Time-resolved images were obtained using an attached FLIM module (Becker & Hickl GmbH, Berlin, Germany) consisting of a time-correlated single photon counting system SPC-150, a GaAsP HPM-100-07 hybrid photodetector, and SPCM software the fluorescence lifetime was measured. NADH fluorescence was isolated using an FB450-40 bandpass optical filter (Thorlabs, USA).

Time-resolved fluorescence images were processed using SPCImage 8.5 software (Becker & Hickl GmbH, Germany). To interpret the time-resolved fluorescence, NADH a_1/a_2 metabolic index was calculated for each pixel of the image, where a_1 and a_2 are amplitudes of the short ($\tau_1 = 0.4$ ns) and long ($\tau_2 = 2.5$ ns) lifetime components of free and bound NADH, respectively [40]. High values of the metabolic index signify the shift of cellular metabolism towards glycolysis, while low values—towards oxidative phosphorylation. In addition to calculating the metabolic index, a phasor diagram approach was applied [41].

Results and discussions

Fluorescence imaging and spectroscopic studies of methylene blue in vivo

Using the video fluorescence imaging, it was shown that after intravenous administration, MB accumulates very quickly (in about 5 seconds) both in the tumor and in normal tissue, Fig. 3.

Then, the intensity of MB fluorescence in normal tissue decreases slightly and remains constant throughout the measurement (5 minutes). In a tumor, on the contrary, a rapid decrease in the MB fluorescence intensity is observed; already after 20 seconds, the luminescence intensity decreases by 4 times relative to the initial value and remains at this level. The obtained time dependences

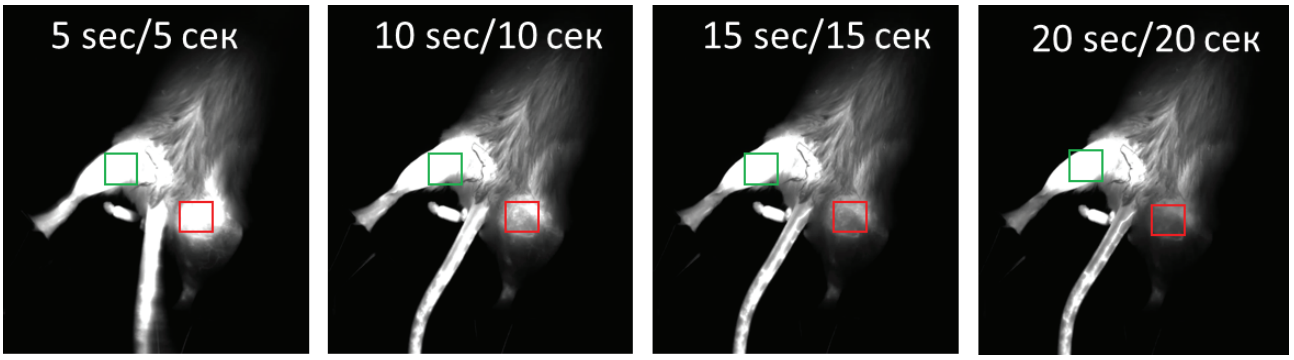

Рис. 3. Флуоресцентная визуализация метиленового синего *in vivo* с использованием возбуждения 660 нм: изображения, полученные через 5, 10, 15 и 20 с после внутривенного введения метиленового синего в дозе 20 мг/кг. Область, выделенная зеленым, соответствует нормальной ткани, область, выделенная красным, – опухоли.
Fig. 3. Fluorescence imaging of MB *in vivo* using 660 nm excitation: images obtained 5, 10, 15 and 20 seconds after intravenous injection MB in 20 mg/kg dose. The area highlighted in green corresponds to normal tissue, the area highlighted in red corresponds to tumor.

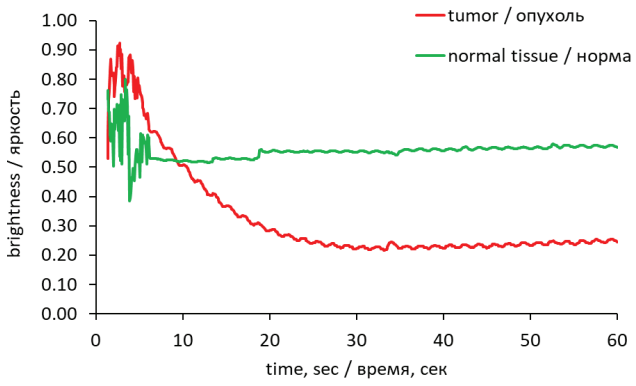

Рис. 4. Зависимости средней яркости для выбранных областей нормальных тканей и опухоли на флуоресцентном изображении от времени.
Fig. 4. Time dependences of the fluorescent image average brightness of selected normal tissue and tumor areas.

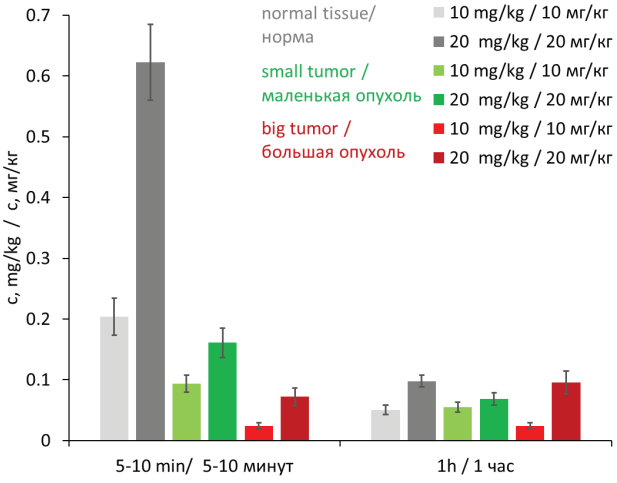

Рис. 5. Концентрация метиленового синего в нормальных тканях и опухоли, определенная спектроскопическими методами через 5 мин и 1 ч после внутривенного введения в дозе 10 и 20 мг/кг.
Fig. 5. The concentration of MB in normal tissues and tumors, determined by spectroscopic methods 5 minutes and 1 hour after intravenous administration at a dose of 10 and 20 mg/kg.

of the average brightness of normal tissue and tumor areas are presented on Fig. 4.

A large spread in fluorescence intensity values in the interval of 2–6 seconds is associated with mouse movement at the moment of MB injection and immediately after. We assume that the observed decrease in the intensity of MB fluorescence is due to the rapid transition to the reduced LMB due to interaction with the components of the tumor microenvironment.

Quantitative assessment of MB accumulation in normal tissue and tumor was carried out using spectroscopic methods by the intensity of fluorescence in the red spectral range, recorded *in vivo*. The dependence of MB concentration on the accumulation time is shown in Fig. 5.

The maximum accumulation in the normal tissue and small tumor was observed 5–10 minutes after injection for both tested concentrations. As expected, the MB cumulative concentration was higher for the higher MB dose. An hour later, the concentration decreased significantly, both in the norm and in a small tumor. For a large tumor, the opposite trend was observed – with an increase in the accumulation time, the MB concentration gradually increased.

To confirm that the decrease in the luminescence intensity of MB is due to the transition to the reduced form of LMB, we studied the absorption of cryosections of normal and tumor tissues *ex vivo*. The absorption spectra recorded using a spectrophotometer are shown in Fig. 6.

The study of the absorption spectra of cryosections *ex vivo* showed the presence of the transition of MB to LMB in the tumor. In the absorption spectrum of normal tissue, an absorption peak is observed in the red region, corresponding to the absorption of the "blue" form. The absorption spectrum of the tumor lacks a peak in the red region, but there is intense absorption in the UV range, presumably corresponding to the absorption of LMB. The absorption peak at a wavelength of 420 nm

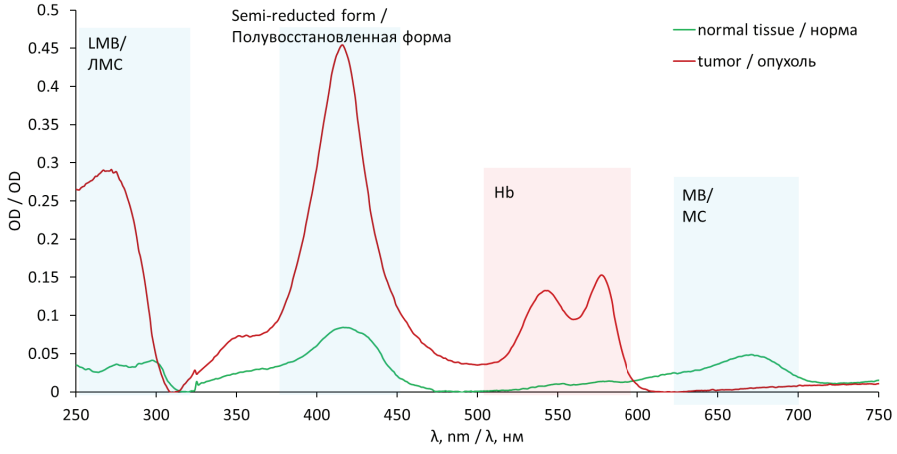

Рис. 6. Спектры поглощения криосрезов нормальных и опухолевых тканей после введения метиленового синего, доза 20 мг/кг (МС – метиленовый синий, ЛМС – лейкометиленовый синий).
Fig. 6. Absorption spectra of normal and tumor tissues cryosections obtained after MB injection, dose 20 mg/kg.

corresponds to the absorption of the semi-reduced form; in the range of 500–600 nm, a characteristic hemoglobin absorption peak is observed for the tumor. Thus, analysis of the absorption spectra makes it possible to study the transition of the main form of MB into its reduced form under the influence of external factors.

Determination of hemoglobin oxygenation level in the tissue microvasculature

Along with assessment of MB accumulation in normal tissue and tumor, the oxygenation level *in vivo* was measured by the hemoglobin absorption. The dependence of tumor oxygenation in relation to normal tissue on the MB accumulation time is shown in Fig. 7.

Prior to the administration of MB, the degree of tumor oxygenation is about 85 and 70% relative to normal tissues for small and large tumors, respectively. In 5–10 minutes after the administration of MB for small tumors, a decrease in the level by 10% is observed, 1 hour after the administration, oxygenation is restored to its original level or exceeds it, depending on the concentration of the drug. 5 hours after the administration of the drug for small tumors, the degree of oxygenation continues to increase and approaches the level of oxygenation of normal tissues (90%). This dependence correlates with the pharmacokinetics of MB in small tumors: after 5 minutes, the maximum accumulation of MB (in the oxidized «blue» form) is observed, after an hour the concentration of the drug decreases.

The dependence of oxygenation of large tissues on time after the introduction of MB has a different character. Initially, oxygenation of large tumors is lower and is about 70% of the norm. 5-10 minutes after the administration of MB, an increase in oxygenation up to 90% is observed, and then oxygenation begins to decrease and is about 65 and 40% 1 and 5 hours after administration, respectively.

According to literature data, MB increases oxygen consumption by tissues with aerobic glycolysis [28]. In this case, oxygen consumption is understood as the amount of oxygen absorbed and used by the body per minute, that is, this is the rate of oxygen use. From the point of view of oxygen consumption, the obtained dependences of the oxygenation on time can be interpreted as follows. For small tumors, MB accumulates rapidly in the tumor and increases oxygen uptake. At the same time, oxygenation of hemoglobin in the microvasculature in the tumor area is reduced. After a while, the concentration of MB decreases and oxygenation begins to increase. At the same time, a temporary increase in oxygen consumption leads to the increase of tumor oxygenation after exposure, which exceeds the initial one. For large tumors, MB accumulation is slower and the concentration accumulated in the tumor is significantly lower than in small tumors (Fig. 5), since the central part of the tumor is poorly supplied with blood. A decrease in oxygenation is observed after a longer time after the administration of the drug (Fig. 7) since more time is required for MB to accumulate in tumor tissues and have an effect. The increase in the oxygenation level after 5–10 minutes can be explained by the positive effect of MB on peripheral blood flow.

Assessment of intracellular metabolism by endogenous NADH photoluminescence lifetime

Time-resolved fluorescence imaging was used to investigate the effect of MB administration on the metabolic type of tumor tissues. Phasor diagrams in the NADH spectral range from tumor slices after MB intravenous injection in 20 mg/kg dose are shown in Fig. 8.

The phasor diagrams of tumors treated with MB show a shift towards shorter lifetimes relative to the control tumor. The NADH a_1/a_2 metabolic index calculated from

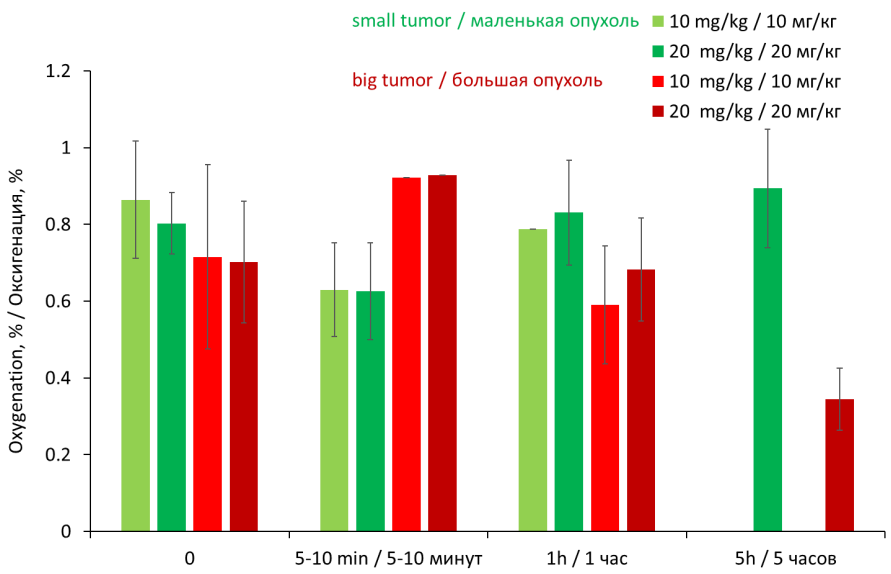

Рис. 7. Степень оксигенации опухоли по отношению к нормальной ткани, определенная по поглощению гемоглобина до, через 5 мин и через 1 ч после внутривенного введения метиленового синего в дозе 10 и 20 мг/кг.
Fig. 7. The oxygenation level of tumor in relation to normal tissue, determined by the hemoglobin absorption before, and 5 minutes and 1 hour after MB intravenous administration at a dose of 10 and 20 mg/kg.

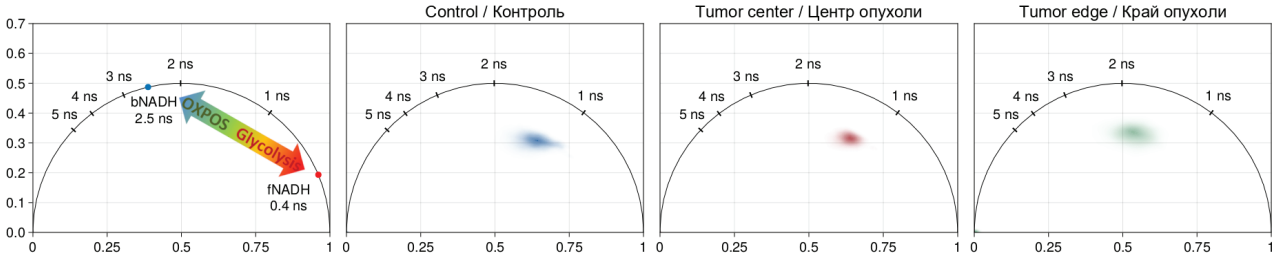

Рис. 8. Фазорные диаграммы разрешенных во времени флуоресцентных изображений NADH в срезах опухоли после внутривенного введения метиленового синего в дозе 20 мг/кг: контроль – опухоль без метиленового синего, центр опухоли – измерение в центре опухоли, край опухоли – измерение на краю опухоли.
Fig. 8. Phasor diagrams for time-resolved fluorescence images of NADH in tumor cryosections after MB intravenous injection in 20 mg/kg dose: control – tumor without MB, tumor center – measurement in the center of the tumor, tumor edge – measurement at the edge of the tumor.

slice images amounted to 8.01±1.84, 7.12±0.87 and 6.65±1.56 for the control tumor without MB, the center and periphery of the tumor with MB, respectively. Such a shift in the metabolic index indicates a change in the type of metabolism from glycolysis to oxidative phosphorylation.

The difference in the results for the center and periphery of the tumor is due to the fact that the blood vessels that deliver oxygen and MB to the tumor, identified in general toward the epithelial surface but not intertwined deep into the tumor bulk [42]. For tumors, there is usually a decrease in the gradient of oxygen and nutrients from the periphery to the center. Thus, for the periphery of the tumor, there is a higher accumulation of MB due to a better blood supply, as well as a better supply of oxygen.

Conclusion

Using fluorescent imaging and spectroscopic methods, the accumulation of MB in tumors *in vivo* was studied, its effect on the hemoglobin oxygenation level in the tissue microvasculature, as well as tumor metabolism, were analyzed.

After intravenous administration, a rapid decrease in the MB fluorescence intensity was observed in the tumor. After 20 seconds, the luminescence intensity decreases by 4 times relative to the initial value and remains at this level. We assume that the observed decrease in the intensity of MB fluorescence is due to the rapid transition to the reduced LMB due to interaction with the components of the tumor microenvironment. This assumption is confirmed by the absorption spectra of cryosections *ex vivo* showing the presence of the transition of MB to LMB in the tumor. Intense absorption in the UV range, presumably corresponding to the absorption of LMB, was observed in the absorption spectrum of the tumor.

For small tumors, MB accumulates rapidly in the tumor and increases oxygen uptake, so the oxygenation of hemoglobin in the microvasculature in the tumor area decreases. When the concentration of methylene blue decreases and oxygenation begins to increase. At the same time, a temporary increase in oxygen consumption leads to the increase of tumor oxygenation after exposure, which exceeds the initial one. For large tumors, MB accumulation is slower, so the decrease in oxygenation is observed after a longer time after the administration of the drug.

The phasor diagrams of tumors treated with MB show a shift towards shorter lifetimes relative to the control tumor. The NADH a_1/a_2 metabolic index calculated from slice images amounted to 8.01±1.84, 7.12±0.87 and 6.65±1.56 for the control without MB, the center and periphery of the tumor with MB, respectively. Such a shift in the metabolic index indicates a change in the type of metabolism from glycolysis to oxidative phosphorylation.

Thus, the use of MB contributes to an increase in oxygen consumption by the tumor, and also leads to a shift in metabolism towards oxidative phosphorylation. We assume that this will positively influence the tumor microenvironment towards tumor regression. Increasing tissue oxygenation with the help of MB will significantly increase the effectiveness of PDT. The results obtained have great potential for practical implementation, as they will significantly increase the effectiveness of modern methods of cancer therapy, especially in relation to tumors in a state of hypoxia that are difficult to treat.

Acknowledgment

The study was funded by a grant from the Russian Science Foundation (project N 22-72-10117).

REFERENCES

1. Bray F., Ferlay J., Soerjomataram I., Siegel R.L., Torre L.A., Jemal A. Global cancer statistics 2018: GLOBOCAN estimates of incidence and mortality worldwide for 36 cancers in 185 countries, *Global cancer statistics*, 2018, 6, pp. 394-424.
2. Biswas S.K., Mantovani A. Macrophage plasticity and interaction with lymphocyte subsets: cancer as a paradigm, *Nature*

ЛИТЕРАТУРА

1. Bray F., Ferlay J., Soerjomataram I., Siegel R.L., Torre L.A., Jemal A. Global cancer statistics 2018: GLOBOCAN estimates of incidence and mortality worldwide for 36 cancers in 185 countries // Global cancer statistics 2018. – № 6. – P. 394-424.
2. Biswas S.K., Mantovani A. Macrophage plasticity and interaction with lymphocyte subsets: cancer as a paradigm // Nature

Immunology, 2010, Vol. 11(10), pp. 889-896.
3. Pranzini E., Pardella E., Paoli P., Fendt S.-M., Taddei M.L. Metabolic Reprogramming in Anticancer Drug Resistance: A Focus on Amino Acids, *Trends in Cancer*, 2021, Vol. 7(8), pp. 682-699.
4. Persi E., Duran-Frigola M., Damaghi M., Roush W.R., Aloy P., Cleveland J.L., Gillies R.J., Ruppin E. Systems analysis of intracellular pH vulnerabilities for cancer therapy, *Nature Communications*, 2018, Vol. 9(1).
5. Chen D., Xie J., Fiskesund R., Dong W., Liang X., Lv J., Jin X., Liu J., Mo S., Zhang T., Cheng F., Zhou Y., Zhang H., Tang K., Ma J., Liu Y., Huang B. Chloroquine modulates antitumor immune response by resetting tumor-associated macrophages toward M1 phenotype, *Nature Communications*, 2018, Vol. 9(1).
6. Wu A.A., Drake V., Huang H.-S., Chiu S., Zheng L. Reprogramming the tumor microenvironment: tumor-induced immunosuppressive factors paralyze T cells, *OncoImmunology*, 2015, Vol. 4(7), pp. e1016700.
7. Huber V., Camisaschi C., Berzi A., Ferro S., Lugini L., Triulzi T., Tuccitto A., Tagliabue E., Castelli C., Rivoltini L. Cancer acidity: An ultimate frontier of tumor immune escape and a novel target of immunomodulation, *Seminars in Cancer Biology*, 2017, Vol. 43, pp. 74-89.
8. Vander Heiden M.G., Cantley L.C., Thompson C.B. Understanding the Warburg Effect: The Metabolic Requirements of Cell Proliferation, *Science*, 2009, Vol. 324(5930), pp. 1029-1033.
9. Colegio O.R., Chu N.-Q., Szabo A.L., Chu T., Rhebergen A.M., Jairam V., Cyrus N., Brokowski C.E., Eisenbarth S.C., Phillips G.M., Cline G.W., Phillips A.J., Medzhitov R. Functional polarization of tumour-associated macrophages by tumour-derived lactic acid, *Nature*, 2014, Vol. 513(7519), pp. 559-563.
10. 2018 Nobel Prize in Physiology or Medicine James pp. Allison and Tasuku Honjo "For their discovery of cancer therapy by inhibition of negative immune regulation"
11. Blaylock R. Cancer microenvironment, inflammation and cancer stem cells: A hypothesis for a paradigm change and new targets in cancer control, *Surgical Neurology International*, 2015, Vol. 6(1), pp. 92.
12. Correia J.H., Rodrigues J.A., Pimenta S., Dong T., Yang Z. Photodynamic Therapy Review: Principles, Photosensitizers, Applications, and Future Directions, *Pharmaceutics*, 2021, Vol. 13(9), pp. 1332.
13. Fleury C., Mignotte B., Vayssière J.-L. Mitochondrial reactive oxygen species in cell death signaling, *Biochimie*, 2002, Vol. 84(2-3), pp. 131-141.
14. Villalpando-Rodriguez G.E., Gibson S.B. Reactive Oxygen Species (ROS) Regulates Different Types of Cell Death by Acting as a Rheostat, *Oxidative Medicine and Cellular Longevity*, 2021, Vol. 2021, pp. 1-17.
15. Kuznetsov V.V. The use of photod ynamic therapy in the domestic oncology (Review of the literature), *Research'n Practical Medicine Journal*, 2016, Vol. 2(4), pp. 98-105.
16. Reshetov I.V., Korenev S.V., Romanko Yu.S. Modern aspects of photodynamic therapy of basal cell skin cancer, *Biomedical Photonics*, 2022, Vol. 11(3), pp. 35-39.
17. Stranadko E.F. Main stages of development of photodynamic therapy in Russia, *Biomedical Photonics*, 2015, Vol. 4(1), pp. 3-10.
18. Panaseykin Y.A., Kapinus V.N., Filonenko E.V., Polkin V.V., Sevrukov F.E., Isaev P.A., Ivanov S.A., Kaprin A.D. Photodynamic therapy treatment of oral cavity cancer in patients with comorbidities, *Biomedical Photonics*, 2023, Vol. 11(4), pp. 19-24.
19. Klimenko V.V., Knyazev N.A., Moiseenko F.V., Rusanov A.A., Bogdanov A.A., Dubina M.V. Pulse mode of laser photodynamic treatment induced cell apoptosis, *Photodiagnosis and Photodynamic Therapy*, 2016, Vol. 13, pp. 101-107.
20. Mansoori B., Mohammadi A., Amin Doustvandi M., Mohammadnejad F., Kamari F., Gjerstorff M.F., Baradaran B., Hamblin M.R. Photodynamic therapy for cancer: Role of natural products, *Photodiagnosis and Photodynamic Therapy*, 2019, Vol. 26, pp. 395-404.
21. Spring B.Q., Rizvi I., Xu N., Hasan T. The role of photodynamic therapy in overcoming cancer drug resistance, *Photochemical & Photobiological Sciences*, 2015, Vol. 14(8), pp. 1476-1491.
22. Brown S.B., Brown E.A., Walker I. The present and future role of photodynamic therapy in cancer treatment, *The Lancet Oncology*, 2004, Vol. 5(8), pp. 497-508.
23. Brooks M.M. The Mechanism of Methylene Blue Action on Blood, *Science*, 1934, Vol. 80(2062), pp. 15-16.

Immunology. – 2010. – Vol. 11. – Macrophage plasticity and interaction with lymphocyte subsets. – № 10. – P. 889-896.
3. Pranzini E., Pardella E., Paoli P., Fendt S.-M., Taddei M.L. Metabolic Reprogramming in Anticancer Drug Resistance: A Focus on Amino Acids // Trends in Cancer. – 2021. – Vol. 7. – Metabolic Reprogramming in Anticancer Drug Resistance. – № 8. – P. 682-699.
4. Persi E., Duran-Frigola M., Damaghi M., Roush W.R., Aloy P., Cleveland J.L., Gillies R.J., Ruppin E. Systems analysis of intracellular pH vulnerabilities for cancer therapy // Nature Communications. – 2018. – Vol. 9. – № 1.
5. Chen D., Xie J., Fiskesund R., Dong W., Liang X., Lv J., Jin X., Liu J., Mo S., Zhang T., Cheng F., Zhou Y., Zhang H., Tang K., Ma J., Liu Y., Huang B. Chloroquine modulates antitumor immune response by resetting tumor-associated macrophages toward M1 phenotype// Nature Communications. – 2018. – Vol. 9. – № 1.
6. Wu A.A., Drake V., Huang H.-S., Chiu S., Zheng L. Reprogramming the tumor microenvironment: tumor-induced immunosuppressive factors paralyze T cells // OncoImmunology. – 2015. – Vol. 4. – Reprogramming the tumor microenvironment. – № 7. – P. e1016700.
7. Huber V., Camisaschi C., Berzi A., Ferro S., Lugini L., Triulzi T., Tuccitto A., Tagliabue E., Castelli C., Rivoltini L. Cancer acidity: An ultimate frontier of tumor immune escape and a novel target of immunomodulation // Seminars in Cancer Biology. – 2017. – Vol. 43. – Cancer acidity. – P. 74-89.
8. Vander Heiden M.G., Cantley L.C., Thompson C.B. Understanding the Warburg Effect: The Metabolic Requirements of Cell Proliferation // Science. – 2009. – Vol. 324. – Understanding the Warburg Effect. – № 5930. – P. 1029-1033.
9. Colegio O.R., Chu N.-Q., Szabo A.L., Chu T., Rhebergen A.M., Jairam V., Cyrus N., Brokowski C.E., Eisenbarth S.C., Phillips G.M., Cline G.W., Phillips A.J., Medzhitov R. Functional polarization of tumour-associated macrophages by tumour-derived lactic acid // Nature. – 2014. – Vol. 513. – № 7519. – P. 559-563.
10. 2018 Nobel Prize in Physiology or Medicine James pp. Allison and Tasuku Honjo "For their discovery of cancer therapy by inhibition of negative immune regulation"
11. Blaylock R. Cancer microenvironment, inflammation and cancer stem cells: A hypothesis for a paradigm change and new targets in cancer control // Surgical Neurology International. – 2015. – Vol. 6. – Cancer microenvironment, inflammation and cancer stem cells. – № 1. – P. 92.
12. Correia J.H., Rodrigues J.A., Pimenta S., Dong T., Yang Z. Photodynamic Therapy Review: Principles, Photosensitizers, Applications, and Future Directions // Pharmaceutics. – 2021. – Vol. 13. – Photodynamic Therapy Review. – № 9. – P. 1332.
13. Fleury C., Mignotte B., Vayssière J.-L. Mitochondrial reactive oxygen species in cell death signaling // Biochimie. – 2002. – Vol. 84. – № 2-3. – P. 131-141.
14. Villalpando-Rodriguez G.E., Gibson S.B. Reactive Oxygen Species (ROS) Regulates Different Types of Cell Death by Acting as a Rheostat // Oxidative Medicine and Cellular Longevity. – 2021. – Vol. 2021. – P. 1-17.
15. Kuznetsov V.V. The use of photod ynamic therapy in the domestic oncology (Review of the literature) // Research'n Practical Medicine Journal. – 2016. – Vol. 2. – № 4. – P. 98-105.
16. Reshetov I.V., Korenev S.V., Romanko Yu.S. Modern aspects of photodynamic therapy of basal cell skin cancer // Biomedical Photonics. – 2022. – Vol. 11. – № 3. – P. 35-39.
17. Stranadko E.F. Main stages of development of photodynamic therapy in Russia // Biomedical Photonics. – 2015. – Vol. 4. – № 1. – P. 3-10.
18. Panaseykin Y.A., Kapinus V.N., Filonenko E.V., Polkin V.V., Sevrukov F.E., Isaev P.A., Ivanov S.A., Kaprin A.D. Photodynamic therapy treatment of oral cavity cancer in patients with comorbidities // Biomedical Photonics. – 2023. – Vol. 11. – № 4. – P. 19-24.
19. Klimenko V.V., Knyazev N.A., Moiseenko F.V., Rusanov A.A., Bogdanov A.A., Dubina M.V. Pulse mode of laser photodynamic treatment induced cell apoptosis // Photodiagnosis and Photodynamic Therapy. – 2016. – Vol. 13. – P. 101-107.
20. Mansoori B., Mohammadi A., Amin Doustvandi M., Mohammadnejad F., Kamari F., Gjerstorff M.F., Baradaran B., Hamblin M.R. Photodynamic therapy for cancer: Role of natural products // Photodiagnosis and Photodynamic Therapy. – 2019. – Vol. 26. – Photodynamic therapy for cancer. – P. 395-404.
21. Spring B.Q., Rizvi I., Xu N., Hasan T. The role of photodynamic therapy in overcoming cancer drug resistance // Photochemical & Photobiological Sciences. – 2015. – Vol. 14. – № 8. – P. 1476-1491.
22. Brown S.B., Brown E.A., Walker I. The present and future role of photodynamic therapy in cancer treatment // The Lancet Oncology. – 2004. – Vol. 5. – № 8. – P. 497-508.
23. Brooks M.M. The Mechanism of Methylene Blue Action on Blood // Science. – 1934. – Vol. 80. – № 2062. – P. 15-16.

24. Brooks M.M. Methylene blue as antidote for cyanide and carbon monoxide poisoning, *JAMA: The Journal of the American Medical Association*, 1933, Vol. 100(1), pp. 59.
25. Wendel W.B. The Mechanism of the Antidotal Action of Methylene Blue in Cyanide Poisoning, *Science*, 1934, Vol. 80(2078), pp. 381-382.
26. Wendel W.B. The control of methemoglobinemia with methylene blue, *Journal of Clinical Investigation*, 1939, Vol. 18(2), pp. 179-185.
27. Chen K.K. Nitrite and thiosulfate therapy in cyanide poisoning, *Journal of the American Medical Association*, 1952, Vol. 149(2), pp. 113.
28. Barron E.S.G. The catalytic effect of methylene blue on the oxygen consumption of tumors and normal tissues, *Journal of Experimental Medicine*, 1930, Vol. 52(3), pp. 447-456.
29. Sevcik P., Dunford H.B. Kinetics of the oxidation of NADH by methylene blue in a closed system, *The Journal of Physical Chemistry*, 1991, Vol. 95(6), pp. 2411-2415.
30. Engbersen J.F.J., Koudijs A., Van Der Plas H.C. Reaction of NADH models with methylene blue, *Recueil des Travaux Chimiques des Pays-Bas*, 2010, Vol. 104(5), pp. 131-138.
31. Schirmer R.H., Adler H., Pickhardt M., Mandelkow E. "Lest we forget you — methylene blue …", *Neurobiology of Aging*, 2011, Vol. 32(12), pp. 2325.e7-2325.e16.
32. Buchholz K., Schirmer R.H., Eubel J.K., Akoachere M.B., Dandekar T., Becker K., Gromer S. Interactions of Methylene Blue with Human Disulfide Reductases and Their Orthologues from Plasmodium falciparum, *Antimicrobial Agents and Chemotherapy*, 2008, Vol. 52(1), pp. 183-191.
33. Komlódi T., Tretter L. Methylene blue stimulates substrate-level phosphorylation catalysed by succinyl–CoA ligase in the citric acid cycle, *Neuropharmacology*, 2017, Vol. 123, pp. 287-298.
34. Zhang H., Rogiers P., Preiser J.-C., Spapen H., Manikis P., Metz G., Vincent J.-L. Effects of methylene blue on oxygen availability and regional blood flow during endotoxic shock:, *Critical Care Medicine*, 1995, Vol. 23(10), pp. 1711-1721.
35. Tepaev R.F., Vishnevskiy V.A., Kuzin S.A., Sergey I.V., Gordeeva O.B., Pytal A.V., Murashkin N.N. Benzocaine-Induced Methemoglobinemia. A Clinical Case, *Pediatric pharmacology*, 2018, Vol. 15(5), pp. 396-401.
36. Peter C., Hongwan D., Küpfer A., Lauterburg B.H. Pharmacokinetics and organ distribution of intravenous and oral methylene blue, *European Journal of Clinical Pharmacology*, 2000, Vol. 56(3), pp. 247-250.
37. Lee S.-K., Mills A. Novel photochemistry of leuco-Methylene Blue, *Chemical Communications*, 2003, 18, pp. 2366.
38. Stratonnikov A.A., Loschenov V.B. Evaluation of blood oxygen saturation in vivo from diffuse reflectance spectra, *Journal of Biomedical Optics*, 2001, Vol. 6(4), pp. 457.
39. Sharick J.T., Favreau P.F., Gillette A.A., Sdao S.M., Merrins M.J., Skala M.C. Protein-bound NAD(P)H Lifetime is Sensitive to Multiple Fates of Glucose Carbon, *Scientific Reports*, 2018, Vol. 8(1), pp. 5456.
40. Kalinina S., Freymueller C., Naskar N., Von Einem B., Reess K., Sroka R., Rueck A. Bioenergetic Alterations of Metabolic Redox Coenzymes as NADH, FAD and FMN by Means of Fluorescence Lifetime Imaging Techniques, *International Journal of Molecular Sciences*, 2021, Vol. 22(11), pp. 5952.
41. Ranjit S., Malacrida L., Jameson D.M., Gratton E. Fit-free analysis of fluorescence lifetime imaging data using the phasor approach, *Nature Protocols*, 2018, Vol. 13(9), pp. 1979-2004.
42. Worth K.R., Papandreou I., Hammond E.M. How the histological structure of some lung cancers shaped almost 70 years of radiobiology, *British Journal of Cancer*, 2023, Vol. 128(3), pp. 407-412.

24. Brooks M.M. Methylene blue as antidote for cyanide and carbon monoxide poisoning // JAMA: The Journal of the American Medical Association. – 1933. – Vol. 100. – № 1. – P. 59.
25. Wendel W.B. The Mechanism of the Antidotal Action of Methylene Blue in Cyanide Poisoning // Science. – 1934. – Vol. 80. – № 2078. – P. 381-382.
26. Wendel W.B. The control of methemoglobinemia with methylene blue // Journal of Clinical Investigation. – 1939. – Vol. 18. – № 2. – P. 179-185.
27. Chen K.K. Nitrite and thiosulfate therapy in cyanide poisoning // Journal of the American Medical Association. – 1952. – Vol. 149. – № 2. – P. 113.
28. Barron E.S.G. The catalytic effect of methylene blue on the oxygen consumption of tumors and normal tissues // Journal of Experimental Medicine. – 1930. – Vol. 52. – № 3. – P. 447-456.
29. Sevcik P., Dunford H.B. Kinetics of the oxidation of NADH by methylene blue in a closed system // The Journal of Physical Chemistry. – 1991. – Vol. 95. – № 6. – P. 2411-2415.
30. Engbersen J.F.J., Koudijs A., Van Der Plas H.C. Reaction of NADH models with methylene blue // Recueil des Travaux Chimiques des Pays-Bas. – 2010. – Vol. 104. – № 5. – P. 131-138.
31. Schirmer R.H., Adler H., Pickhardt M., Mandelkow E. "Lest we forget you — methylene blue …" // Neurobiology of Aging. – 2011. – Vol. 32. – № 12. – P. 2325.e7-2325.e16.
32. Buchholz K., Schirmer R.H., Eubel J.K., Akoachere M.B., Dandekar T., Becker K., Gromer S. Interactions of Methylene Blue with Human Disulfide Reductases and Their Orthologues from Plasmodium falciparum // Antimicrobial Agents and Chemotherapy. – 2008. – Vol. 52. – № 1. – P. 183-191.
33. Komlódi T., Tretter L. Methylene blue stimulates substrate-level phosphorylation catalysed by succinyl–CoA ligase in the citric acid cycle // Neuropharmacology. – 2017. – Vol. 123. – P. 287-298.
34. Zhang H., Rogiers P., Preiser J.-C., Spapen H., Manikis P., Metz G., Vincent J.-L. Effects of methylene blue on oxygen availability and regional blood flow during endotoxic shock // Critical Care Medicine. – 1995. – Vol. 23. – № 10. – P. 1711-1721.
35. Tepaev R.F., Vishnevskiy V.A., Kuzin S.A., Sergey I.V., Gordeeva O.B., Pytal A.V., Murashkin N.N. Benzocaine-Induced Methemoglobinemia. A Clinical Case // Pediatric pharmacology. – 2018. – Vol. 15. – № 5. – P. 396-401.
36. Peter C., Hongwan D., Küpfer A., Lauterburg B.H. Pharmacokinetics and organ distribution of intravenous and oral methylene blue // European Journal of Clinical Pharmacology. – 2000. – Vol. 56. – № 3. – P. 247-250.
37. Lee S.-K., Mills A. Novel photochemistry of leuco-Methylene Blue // Chemical Communications. – 2003. – № 18. – P. 2366.
38. Stratonnikov A.A., Loschenov V.B. Evaluation of blood oxygen saturation in vivo from diffuse reflectance spectra // Journal of Biomedical Optics. – 2001. – Vol. 6. – № 4. – P. 457.
39. Sharick J.T., Favreau P.F., Gillette A.A., Sdao S.M., Merrins M.J., Skala M.C. Protein-bound NAD(P)H Lifetime is Sensitive to Multiple Fates of Glucose Carbon/ / Scientific Reports. – 2018. – Vol. 8. – № 1. – P. 5456.
40. Kalinina S., Freymueller C., Naskar N., Von Einem B., Reess K., Sroka R., Rueck A. Bioenergetic Alterations of Metabolic Redox Coenzymes as NADH, FAD and FMN by Means of Fluorescence Lifetime Imaging Techniques // International Journal of Molecular Sciences. – 2021. – Vol. 22. – № 11. – P. 5952.
41. Ranjit S., Malacrida L., Jameson D.M., Gratton E. Fit-free analysis of fluorescence lifetime imaging data using the phasor approach// Nature Protocols. – 2018. – Vol. 13. – № 9. – P. 1979-2004.
42. Worth K.R., Papandreou I., Hammond E.M. How the histological structure of some lung cancers shaped almost 70 years of radiobiology // British Journal of Cancer. – 2023. – Vol. 128. – № 3. – P. 407-412.